Dynamic ordering and instability of the vortex lattice in Nb films exhibiting moderately strong pinning

G. Grimaldi,[1,*] A. Leo,[1] A. Nigro,[1,2] S. Pace,[1,2] and R. P. Huebener[3]
[1]*Laboratorio Regionale SuperMat, CNR–INFM, Salerno I-84081, Italy*
[2]*Dipartimento di Fisica "E R Caianiello," Università di Salerno, Via Salvador Allende, Baronissi, I-84081 Salerno, Italy*
[3]*Physikalisches Institut, Universitaet Tuebingen, D-72076 Tuebingen, Germany*
(Received 22 July 2009; revised manuscript received 15 September 2009; published 21 October 2009)

We study the nonlinear effects in the current-voltage characteristics of Nb superconducting thin films, induced both by the current dependence of the pinning force and by the electric-field dependence of the flux-flow resistance of Abrikosov vortices driven by high electric currents. Despite of the quite strong pinning in our samples, by increasing the bias current, in a temperature dependent magnetic-field range, the moving vortex system undergoes a dynamical transition from a disordered to an ordered vortex lattice. Such transition leads to a quite sharp reduction of the dynamic pinning force corresponding to a peak in the current dependence of the differential flux-flow resistance. On the same samples, in a higher voltage-velocity regime, for a different temperature dependent magnetic-field range, an instability of the moving vortex lattice also occurs, with a sudden jump in the *I-V* curve from the non linear flux-flow branch to the linear normal resistive state. Within the Larkin-Ovchinnikov velocity dependence of the flux-flow resistance, this flux-flow instability has been studied as function of the magnetic field and temperature in order to get out its nonequilibrium electronic nature. Finally, we propose a dynamic phase diagram to describe the vortex lattice motion driven by high electric currents in the presence of such a disordered pinning landscape.

DOI: 10.1103/PhysRevB.80.144521 PACS number(s): 74.25.Fy, 74.25.Qt, 74.78.Db, 74.25.Sv

I. INTRODUCTION

In type-II low temperature superconductors (LTS) the linear flux-flow motion of the Abrikosov vortex lattice is a prominent feature corresponding to a linear current-voltage characteristic (IVC) either in the absence of pinning or above the superconducting critical current I_c.[1] Indeed for homogeneous samples the *I-V* curve is written as $V=R_F(I-I_c)$, that for $I>I_c$ implies a linear behavior if the pinning force and the flux-flow resistance R_F are current independent. In this case the usual picture given by Bardeen-Stephen (BS) yields the well known flux-flow resistance $R_F=R_{BS}=(N\Phi_0/B_{c2})R_n$,[2] usually in agreement with experimental data,[3] which underlines that the total number of vortices $N=B/\Phi_0$ is moving with the same flux-flow velocity and that the local magnetic induction B is constant in the sample and equal to the applied one. The BS dependence is valid in the case of the dirty limit, where the electronic quantum structure of the vortices is smeared due to the small value of the mean electronic scattering time τ.[4]

On the other hand, discrepancies from the linear behavior can arise from the electric-field dependence of the flux-flow resistance[5] or due to an inhomogeneous distribution of the critical current density.[6] Here, nonlinearities close to the critical current due to thermal activation processes are not considered; as well as Joule heating processes at high currents can be minimized. Nonlinearity of IVC can be ascribed to a decreasing of the mean pinning force F_p with increasing current (with the consequent increase of the vortex velocity) accompanied by a change of the moving vortex lattice induced by the bias current. In fact due to the competition between the elasticity of the vortex-vortex interaction and the strength of the vortex-pin interaction in the presence of disorder, owing to the underlying pin distribution, the vortex lattice deforms to adapt itself to the pinning centers. Thus the resulting average pinning force F_p depends on this rearrangement of the vortex lattice. In the strong pinning case, each vortex feels the single interaction f_p with a pinning center and the correlations among all the other vortices become weak, thus the flux line lattice breaks into clusters with finite correlation lengths. On the contrary, in the weak-pinning case, the vortex lattice undergoes a smooth elastic perturbation, so that a collective interaction is established, with a further reduction of the average pinning force F_p and an homogeneous moving vortex lattice. As a consequence, by varying the external magnetic field and temperature, a tuning from one to the other case can be obtained. This vortex lattice changing behavior is responsible for the so-called peak effect (PE) of the critical current,[7] which can lead to a transition of the vortex lattice from an ordered phase to a disordered one. Very recently, it has been outlined that the origin of the PE is still under debate, indeed it has been clarified that such effect strongly depends on the pinning mechanism.[8–10] Moreover, since the total pinning force can also depend on the bias current, a dynamical transition, known as dynamic ordering (DO), driven by an increasing bias current may occur from the disordered plastic phase which usually shows a higher F_p to an ordered one, marked by a lower F_p. In presence of strong spatial pinning inhomogeneity, the disordered phase can give rise to a distribution of pinning forces leading in some cases to easy flux-flow channels or to vortex shearing.[11] The change in the vortex motion from a plastically disordered flow to a more ordered elastic motion, i.e., dynamic ordering,[12] related to the reduction of the mean pinning force, corresponds to the presence of a peak in the differential resistance $R_d=dV/dI$. Such a peak occurs at a definite value of the bias current, which strongly depends on the magnetic field and temperature for a certain

degree of disorder in the sample.[12–14] In the past much attention has been focused on the current induced ordering of vortices in weak-pinning superconducting materials. Indeed, the change of slope in the IVC, with the corresponding peak in the differential resistance R_d versus I, has been widely studied in weak-pinning samples, such as 2H-$NbSe_2$ single crystals,[15] $Nb_{70}Ge_{30}$ thin films,[13] $Mo_{77}Ge_{23}$ thin films,[16] $Mo_{75}Re_{25}$ thin films.[17] Experimental studies,[13,15,18–20] theoretical works,[12,21] and computer simulations[14,22–24] have confirmed that such a peak is determined by the dynamic phase transition of the vortex lattice from the plastically (disordered) to the elastically (ordered) flow.

In addition to DO, intrinsic electronic nonequilibrium effects in the mixed state lead to highly nonlinear behavior, as predicted by Larkin and Ovchinnikov (LO) more than 30 years ago.[25] Advances in thin-film technology allow the fabrication of superconducting film specimens with a thickness approaching the nm range. Due to the corresponding strong increase in the surface-to-volume ratio, Joule heating effects in the presence of an applied electric current can be considerably reduced, and nonequilibrium processes can be studied more accurately. In the past, electronic nonequilibrium phenomena have been observed in two classes of materials: semiconductors and superconductors in the mixed state. In both cases it is the relatively small concentration of the relevant charge carriers, which allows the generation of an appreciable electric field in the sample without resulting in an electric current of such magnitude that Joule heating becomes the dominating nonequilibrium effect. We note that in this context in the mixed state of superconductors the relevant charge carriers are the quasiparticles and not the superconducting Cooper pairs. In contrast to this, in a metallic conductor the high value of the dissipative electric current usually results in a dominating influence of Joule heating effects.

For the study of electronic nonequilibrium effects in the mixed state of a type-II superconducting film it is clearly beneficial if the substrate of the superconducting film shows a high value of the thermal conductivity, and if the film/substrate configuration is embedded directly within liquid or even superfluid helium. The nonequilibrium LO theory refers to the situation where the vortex lattice generated by an applied magnetic field is set into motion due to the Lorentz force induced by an applied electric current. In the temperature range not too far below the critical temperature T_c, the energy supplied in the core to the quasiparticles by the electric field is sufficient to let them escape from the core itself, determining a nonequilibrium distribution of the quasipartciles.

LO derived the following expression for the flux-flow resistivity ρ_F,[25]

$$\rho_F(E) = \rho_F(0)\left[1 + \left(\frac{E}{E^*}\right)^2\right], \tag{1}$$

where E is the flux-flow electric field and $\rho_F(0)$ refers to the limit $E=0$. Equation (1) states that the flux-flow resistivity becomes electric-field dependent. The resulting IVC show an upward curvature, and negative differential resistivity sets in at $E=E^*$. In the case of current-biased operation, at $E=E^*$ the resistive voltage jumps discontinuously to a higher value, inducing a flux-flow instability (FFI). We note that the critical electric field E^* and the critical vortex velocity v^* are related by means of the equation $\mathbf{E}^*=\mathbf{B}\times\mathbf{v}^*$, where $\mathbf{B}$ is the magnetic flux density. Therefore the relation between the predicted critical vortex velocity and the experimental critical voltage V^* is given by $v^*(B)=V^*/BL$, where, for an homogeneous vortex motion, L is the distance between the voltage contacts.

The quantity v^* is given by the LO theory[25]

$$v^* = \sqrt{\frac{(1-T/T_c)^{1/2}D[14\zeta(3)]^{1/2}}{\pi\tau_\epsilon}}. \tag{2}$$

Here D is the quasiparticle diffusion coefficient, $\zeta(x)$ is the Riemann zeta function, and τ_ϵ is the quasiparticle energy relaxation time. The quasiparticle system tends to relax back to its equilibrium distribution with the rate τ_ϵ^{-1}.

In this paper we report on the DO and FFI effects of the vortex motion in superconducting thin Nb films with quite strong flux pinning. The critical vortex velocity v^* which

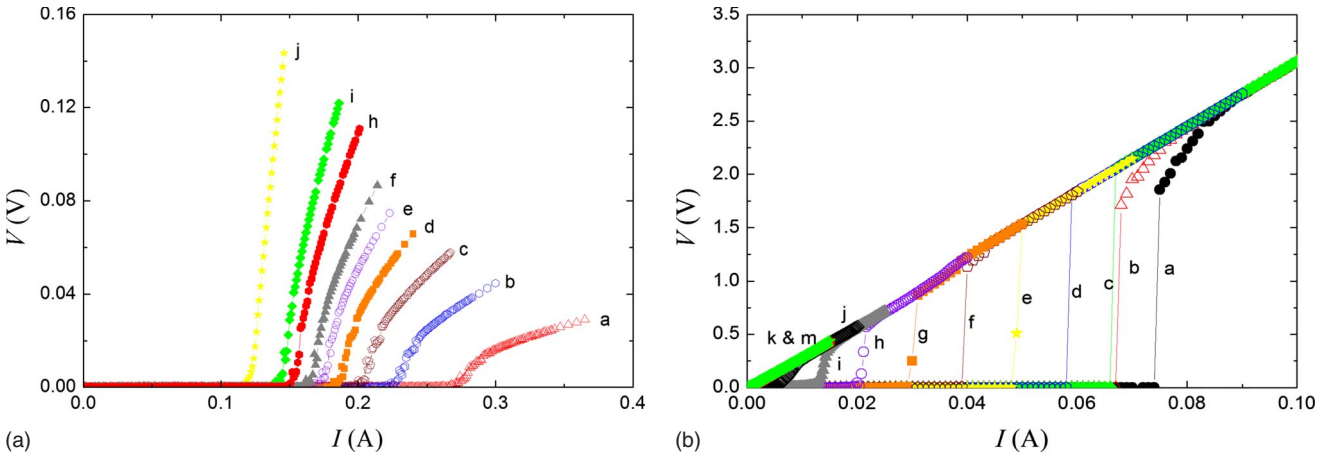

FIG. 1. (Color online) (a) IV at $T=2.1$ K in a low field range: a=0.01, b=0.02, c=0.03, d=0.04, e=0.05, f=0.06, h=0.08, i=0.1, j=0.2 T. (b) IV at $T=2.1$ K in a high field range. The curves are shown starting from a=1.0 T to m=3.2 T with a magnetic-field step of 0.2 T.

TABLE I. Physical parameters of the Nb films.

Parameter	Value
Film thickness d	0.1 μm
Electron mean free path l_f	5 nm
Fermi velocity v_F	2×10^5 m/s
Coherence length at zero temperature $\xi(0)$	7 nm
Normal state resistivity ρ_{10K}	15 $\mu\Omega$ cm

could be ascribed to the flux-flow instability, as predicted by LO,[25] was measured as a function of the magnetic field and the temperature. In addition, before the instability was reached, a peak in the electric current dependence of the differential flux-flow resistance was also observed corresponding to the dynamic ordering transition. To our knowledge, this is the first time that such a nonlinear effect was observed in the presence of quite strong pinning, close to the vortex velocity instability.

II. EXPERIMENTAL RESULTS

The samples investigated were Nb thin films with 100 nm thickness deposited on Si(100) substrates in a UHV dc diode magnetron sputtering system, with a base pressure of about 4×10^{-8} mbar and a sputtering argon pressure of 10^{-3} mbar. The deposition rate was typically 0.28 nm/s. It was controlled by a quartz crystal monitor calibrated by low-angle reflectivity measurements. The Nb strips were 100 μm wide and 2 mm long. The typical superconducting transition temperature was $T_c=8.5$ K with a transition width $\Delta T_c=0.1$ K. The residual resistance ratio was always around $R(300\ \mathrm{K})/R(10\ \mathrm{K})\approx2$. A typical value of the critical current density, obtained by the standard 10 μV/cm criterion, at 4.2 K and zero magnetic field was $J_c=2\times10^6$ A/cm^2. The Nb films are type-II superconductors having a Ginzburg-Landau parameter $\kappa\approx6$. The characteristic sample parameters are summarized in Table I.

The transport measurements were performed using the four-point configuration in the presence of an external magnetic field up to 3 T applied perpendicular to the film plane and in the temperature range between 2.1 K and T_c. At temperatures of 4.2 K and below the samples were always in direct contact with liquid helium. The lower values of the magnetic field were generated using a copper coil having a field/current ratio of 0.013 T/A. In order to minimize Joule heating effects, the IVCs were measured using rectangular current pulses with a current-on time of 2.5 ms and a current-off time of 3.5 ms. During the pulsed measurements the sample temperature was continuously monitored, and by sweeping the pulse height of the bias current upward and downward no hysteresis has been observed so that thermal effects can be excluded.

In Figs. 1(a) and 2(a) we show the measured IVCs at different applied magnetic fields at the temperature of 2.1 K in superfluid helium and at 4.2 K, respectively. The magnetic-field values are indicated in the caption of the figures. At their upper ends the curves jump to higher voltages. This occurs at a critical voltage V^*, as can be seen in Figs. 1(b) and 2(b). As we see from Figs. 1(a) and 2(a), in a definite temperature dependent field range, before the instability is reached, a change of the curve concavity is observed which can be related to the presence of a peak in the differential resistance dV/dI. Above the peak an almost linear IVC is recovered, implying a current independent dynamic pinning force and a constant flux-flow resistance, almost in agreement with the BS prediction. In order to demonstrate this effect more clearly, the derivatives dV/dI of the IVC's were calculated numerically from the data, and they are plotted versus the applied electric current in Fig. 3 in which part (a) refers to the temperature of 2.1 K and part (b) to 4.2 K. The peak in the differential resistance dV/dI can clearly be seen, and at 2.1 K this effect is more pronounced than at 4.2 K. This nonmonotonic behavior of the derivative dV/dI is likely due to the influence of flux pinning, as will be discussed in the next section.

We remark that, above the peaks, the asymptotic values of the differential resistances shown in Figs. 3(a) and 3(b) are

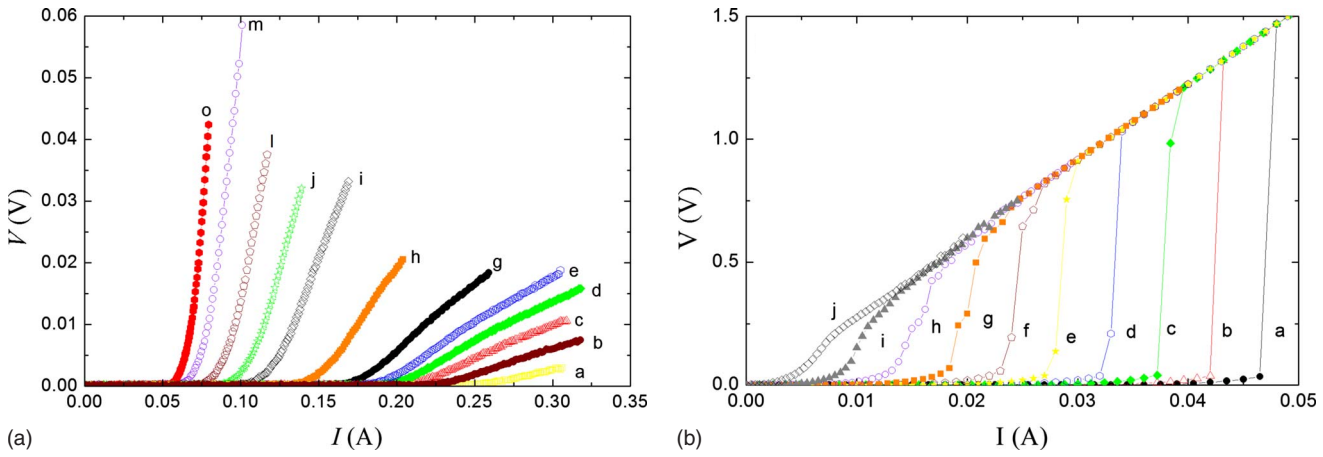

FIG. 2. (Color online) (a) IV at $T=4.2$ K in a low field range: a=0.003, b=0.004, c=0.005, d=0.006, e=0.008, g=0.01, h=0.02, i=0.04, j=0.06, k=0.08, l=0.1, m=0.2, o=0.4 T. (b) IV at $T=4.2$ K in a high field range, up to B_{c2}. The curves are shown starting from a=1.1 T to j=2.0 T with a magnetic-field step of 0.1 T.

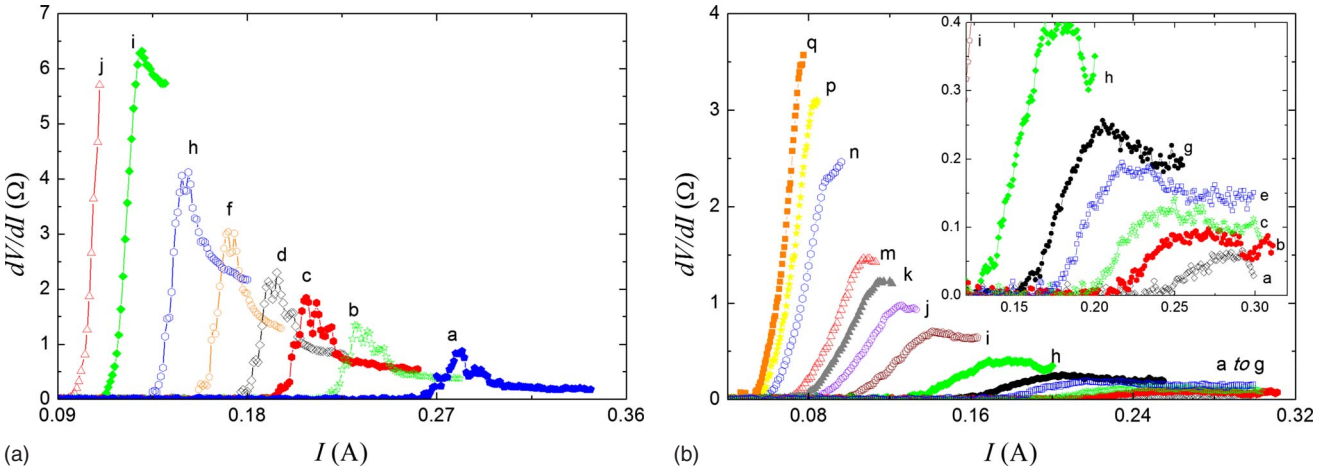

FIG. 3. (Color online) (a) dV/dI at $T=2.1$ K for different magnetic-field values: a=0.01, b=0.02, c=0.03, d=0.04, f=0.08, h=0.2, i=0.4, j=0.5 T. (b) dV/dI at $T=4.2$ K for different magnetic-field values: a=0.003, b=0.004, c=0.005, e=0.007, g=0.01, h=0.02, i=0.04, j=0.06, k=0.08, m=0.1, n=0.2, p=0.3, q=0.4 T. Inset: enlargement of the low field range differential resistance.

the flux-flow values R_F, whereas such peaks correspond to the inflection points in the S-shaped flux-flow branches of the I-V characteristics displayed in Figs. 1(a) and 2(a) at low fields. On the contrary, at higher fields close to B_{c2}, where there are no voltage jumps anymore, the S-shaped I-V curves shown in Figs. 1(b) and 2(b) correspond to the continuous transition to the normal state resistance R_n.

Concerning the observed voltage jumps in the IVC shown in Figs. 1(b) and 2(b) and the instability mechanisms responsible for them, it is important to evaluate the Joule heating effects, in order to see whether they can be definitely neglected.

To distinguish between an extrinsic or intrinsic instability induced at high driving currents, a previous thermal diffusion analysis has been performed to exclude the Joule heating effects, as well as a proper experimental biasing operation mode has been found.[26,27] On that basis we can state that in our Nb thin films the thermal diffusion characteristic time $\tau_T=d^2/\pi^2 D_T=0.04$ ns (D_T is the thermal diffusivity) is much lower than the surface cooling characteristic time by the liquid helium $\tau_h=\gamma Cd/2h=10$ μs (γ is the material density, C is the specific heat, h is the heat transfer coefficient), at least at $T=4.2$ K. These results ensure a uniform temperature across the Nb conductor, but the thermal exchanges with the environment should be evaluated. We already indicated that both the thermal exchanges with the liquid helium bath and with the substrate are involved, due to the finite heat removal rate.[26] In any case the heat transfer coefficient h for liquid helium is high enough ($\approx 10^4$ W/m^2 K), as for the superfluid helium ($\approx 10^5$ W/m^2 K), that the cryogenic stabilization criterion is satisfied in terms of the Stekly parameter,[28]

$$\alpha = \frac{\rho_N J_c^2 d}{h(T-T_0)} \ll 1, \tag{3}$$

where ρ_N is the normal state resistivity, T_0 is the liquid helium bath temperature, and T is the sample temperature. In the Eq. (3), the value is $\alpha=0.002$, as previously estimated in our Ref. 26.

Moreover, by still taking into account the quasiparticle heating, following the theory of Bezuglyj and Shklovskij,[29] we have also already evaluated the critical parameter $B_T=0.24$ T, below which relevant heating effects can be ignored.[26,30] More importantly, on the basis of the experimental evidence on the magnetic field dependence of the dissipated power at the instability point $P^*(B)=I^*V^*$ (as reported elsewhere, see Fig. 2 of Ref. 26, and Fig. 3 of Ref. 31) we became confident that, in the whole magnetic-field range investigated, the observed instabilities should be accounted for intrinsic mechanisms rather than thermal effects.

Therefore, Joule heating effects can be neglected in the isothermal measurements at $T=4.2$ K and 2.1 K.

III. DYNAMIC ORDERING

A. I-V characteristics

At the beginning of our discussion we point out that the Nb films display relatively strong flux pinning due to the large J_c values and to the magnetic-field dependence of the pinning force which is placed in between the weak and the strong pinning behavior. In particular, by a direct comparison of the experimental curves of $F_p(B)$ with the theoretical ones[32] we can identify the type of pinning in our samples as an intermediate regime between weak and strong.[33] For a comparison, well annealed Nb foils of 18 μm thickness, studied by one of the authors almost 40 years ago,[3] at 4.2 K and magnetic fields of 0.1–0.2 T showed a critical current density of about $0.7-2.0\times 10^2$ A/cm^2, i.e., values smaller by four orders of magnitude than those of the present samples. Furthermore, in those Nb foils[3] a residual resistance ratio $R(295\ \text{K})/R(4.2\ \text{K};\ 0.4\ \text{T})=620$ had been measured.

In contrast to the results shown in Figs. 1–3 the homogeneous Nb foils show a pure linear flux-flow behavior $V=R_F(I-I_c)$, this means a direct proportionality of the vortex velocity to the bias current: $v=(R_F/BL)(I-I_c)$, with R_F values in agreement with the BS prediction,[3] corresponding to

the absence of the peak in the derivative dV/dI. We conclude that in our case the peak in the derivative dV/dI is likely caused by pinning effects on magnetic flux quanta. It can be understood in terms of the following considerations.

In the case of dynamic ordering, in the ordered phase the vortex lattice moves as a whole object with a defined pinning force (i.e., a well defined I_c). On the contrary, in the disordered phase, due to a strong spatial variation of the pinning force, the vortices are correlated only within each independent cluster. The actual behavior depends on the inhomogeneity of the pinning centers so that the unit volume pinning force acting on each cluster can be different, leading to a distribution of critical current density. By considering the sample consisting of different slices in series along its length L on the x axis, the critical current density distribution determines different values of the critical current $I'=I_c(x)$ of each slice.[34] Therefore, due to the distribution $f(I')$ of the local critical currents along the sample length, as the bias current increases above each threshold I', vortices are set in motion in the corresponding slice, and this leads to an increasing fraction $n(I)$ of moving vortices as the current increases $n(I)=\int_0^I f(I')dI'$,[6,35] where $n(I)$ is normalized to the total number of vortices N. As a consequence the nonlinear I-V characteristic shows no peak in the differential resistance. Thus, even in the absence of the dynamic ordering, in the presence of inhomogeneity of the pinning centers the vortex velocity can be written,[35]

$$v = \frac{R_F}{BL}\int_0^I (I-I')f(I')dI',$$

where $f(I')$ is the critical current density distribution function, whose details depend on the actual behavior of the pinning centers, although it is often selected a Gaussian distribution function.[6,35]

For large inhomogeneity some vortices can be almost free and move along channels whose number and width can increase with increasing bias current (vortex shearing). The spatial distribution of vortex velocities, in this plastic flow regime has been numerically evaluated by Faleski *et al.*[14] A two-peaks distribution function of the vortex velocity has been obtained allowing to identify two types of vortices: slow vortices associated to the peak centered at the lower velocity and fast vortices associated to the higher velocity peak. Within this scenario the slow vortices are located in the strongly pinned clusters, while fast vortices flow in the channels around the pinned clusters. Hence, only a certain fraction $n_s(I)$ of the total number $n(I)$ of magnetic flux quanta per unit area, which depends on the electric current I, participates in the resistive flux-flow process with a slower vortex velocity (due to a larger pinning force).[14] Thus the difference $n_f(I)=n(I)-n_s(I)$ is the remnant fraction of flux quanta moving with a faster vortex velocity (due to a lower pinning force).

By increasing the driving current, the dynamic ordering of the slow vortices takes place, with the consequent reduction of the experienced pinning force, so that the number of fast vortices increases rapidly leading to a non linear IVC and to a peak in the differential resistance at a given bias current I_p.

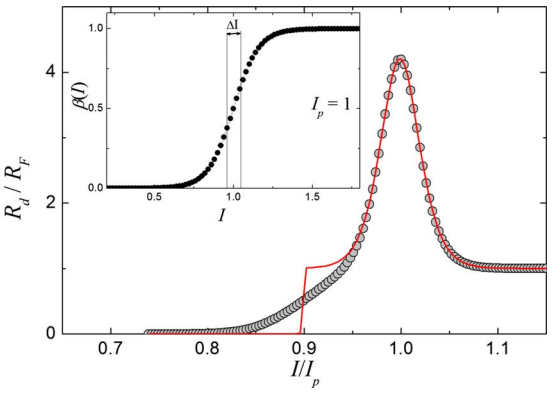

FIG. 4. (Color online) The normalized differential resistance as function of increasing driving current. The solid line is the homogeneous case with a steplike increase corresponding to a definite critical current value. The circles represent numerical data in the case of a Gaussian distribution of critical currents. Inset: the β function versus the driving current. The peak current value I_p and the width ΔI are also displayed (see text).

In other words, within some current range, the vortex lattice undergoes the transition from a disordered phase, corresponding to a larger pinning force, to an ordered phase, corresponding to a lower one. In this case, the effective fraction of vortices, participating in the flux motion with higher velocities, increases, while the number of slower vortices decreases. Therefore, the spatial velocity distribution depends on the bias current I. In particular the relative weight of the two peaks changes as function of I. The average drift velocity of the vortex lattice can be written in terms of the equivalent critical current distribution $f_{DO}(I,I')$,

$$v_d(I) = \frac{R_F}{BL}\int_0^I (I-I')f_{DO}(I,I')dI' \tag{4}$$

with $f_{DO}(I,I')=(1-\beta(I))f_{slow}(I')+\beta(I)f_{fast}(I')$ and $f_{slow,fast}(I')=\frac{C_{s,f}}{\sigma_{s,f}\sqrt{2\pi}}\exp[-\frac{(I'-I_{s,f})^2}{2\sigma_{s,f}^2}]$. The $\beta(I)$ function increases from zero up to 1 and is centered on the peak current value I_p, as shown schematically in Fig. 4 (see inset). Although its particular expression is not strictly relevant to obtain the R_d peak displayed in Fig. 4, thus influencing only its shape (width and height), the $\beta(I)$ function determines the variation of the f_{DO} from the two-peaks distribution $[f_{slow}(I'),f_{fast}(I')]$ to a single peak distribution $[f_{fast}(I')]$ of the ordered phase.

Considering that the mean value I_f is lower than I_s, and that in the ordered phase the width of the distribution function associated with the fast vortices is smaller than the distribution width associated with the slow vortices, since the vortex lattice moves as a whole, the Eq. (4) can be rewritten, for $I>I_f$, as

$$v_d(I) = [1-\beta(I)]\frac{R_F}{BL}\int_0^I (I-I')f_{slow}(I')dI' + \beta(I)\frac{R_F}{BL}(I-I_f). \tag{5}$$

By writing Eqs. (4) and (5) we have retained as starting point the inhomogeneous sample and we added the dynamic ordering ingredient by assuming a different distribution function

depending on the type of moving vortices in the system. Thus, behind Eqs. (4) and (5) the physical meaning is that we are describing the motion of a vortex lattice characterized by an average drift velocity v_d, driven by an increasing bias current which induces an increasing order into the moving vortex system in the presence of an overall inhomogeneous distribution of pinning forces.

Therefore, the full *I-V* curve describing the transition between the two phases can be written as

$$V(I) = [1 - \beta(I)]V_s(I) + \beta(I)V_f(I) \tag{6}$$

with the overall voltage $V=BLv_d$. This implies that the component of the slowly moving vortices should give the overall voltage determined by the critical current distribution: $V_s = R_F\int_0^I (I-I')f_{slow}(I')dI'$.

However, as the current increases, an increasing fraction of slow vortices achieves the ordered state. Once the ordered phase has been completely established, no critical current distribution exists anymore: $V_f=R_F(I-I_f)$.

The resulting current dependence of the differential resistance, plotted in Fig. 4, is

$$R_d = \frac{dV}{dI} = R_F[1 - \beta(I)]\int_0^I f_{slow}(I')dI' + R_F\beta(I) + \frac{d\beta}{dI}(V_f - V_s) \tag{7}$$

where $\frac{dV_s}{dI}=R_F\int_0^I f_{slow}(I')dI'$ and $\frac{dV_f}{dI}=R_F$.

From Eq. (7) it clearly appears that the peak of the differential resistance, shown in Fig. 4, is due to the presence of a peak of $d\beta(I)/dI$. This can lead to the peak of the experimental data shown in Fig. 3. The solid line in Fig. 4 represents the differential resistance with an homogeneous critical current value, and a consequent steplike function. Indeed, in the presence of artificial channels inducing easy flow vortex motion along the channels with a shear interaction among them, it has been recently observed a two steps differential resistance, as shown in Fig. 2 of Kokubo *et al.*[36] In our case the presence of the critical currents distribution leads to the smooth increase of the dynamic flux-flow resistance, whose value is still lower than the Bardeen-Stephen prediction till the DO sets in.

The *I-V* curve of Eq. (6) is displayed in Fig. 5, showing the nonlinear S-shape of the curve (solid red curve) corresponding to the peak of the dynamical resistance. In Fig. 5 the full circles represent the experimental data of the *I-V* at $H=0.02$ T and $T=2.1$ K. The solid red curve is the numerical result obtained from Eq. (6) with the R_F (see inset of Fig. 5) and the I_f parameters fixed by the linear fit at high currents, and the Gaussian free parameters σ_s and I_s. There are two parameters left in the $\beta(I)$ function (see inset of Fig. 4) that determine the range of the bias current in which the DO takes place: the peak current value I_p is fixed by the experimental data and the width ΔI is a free parameter.

B. B-T phase diagram

In agreement with the above discussion, we note that the experimental curves of the *I-V* and dV/dI display the same

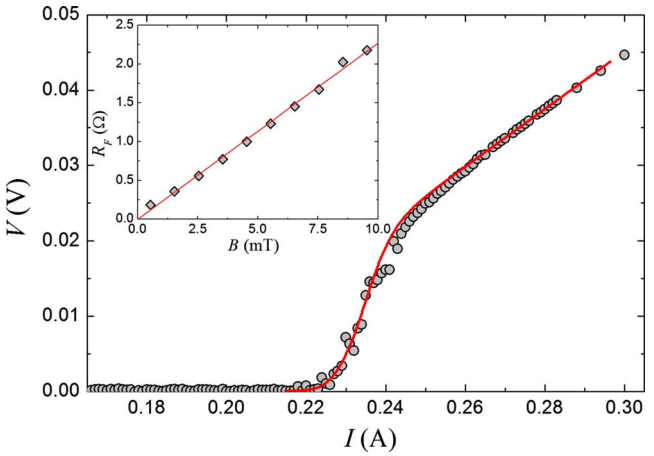

FIG. 5. (Color online) The experimental data (circles) compared to the *I-V* curve numerically calculated (solid red curve) at $B=0.02$ T and $T=2.1$ K. The chosen numerical parameters are: $\sigma_s=0.0025$ A, $I_s=0.225$ A, $I_p=0.235$ A and $\Delta I=0.003$ A. Inset: the flux-flow resistance, deduced by the high current linear fit of the *I-V* curves, as function of the magnetic field.

remarkable features in a limited temperature and magnetic-field range. In particular the observation of a peak in the current dependence of the flux-flow dynamic resistance R_d, displayed in Fig. 3, is shown in the B-T plane in the grayed area of Fig. 6.

By comparing the B-T phase diagram of our Nb thin films with those of weakly and moderately weak-pinning systems, such as Nb-Ge and Mo-Re thin films, respectively,[13,17] we note that for the fairly strong pinning Nb sample, DO already occurs at very low fields of a few mT. This is in agreement with the statement that an increase of the disorder pulls down the lower limit of the magnetic-field range in which DO takes place.[13]

We also outline that the upper limit of the DO magnetic-field range shown in Fig. 6 is placed very far from the melting line as well as the B_{c2} line of such Nb low temperature superconductor. Therefore our data are consistent with the dynamic ordering interpretation, although there is no evi-

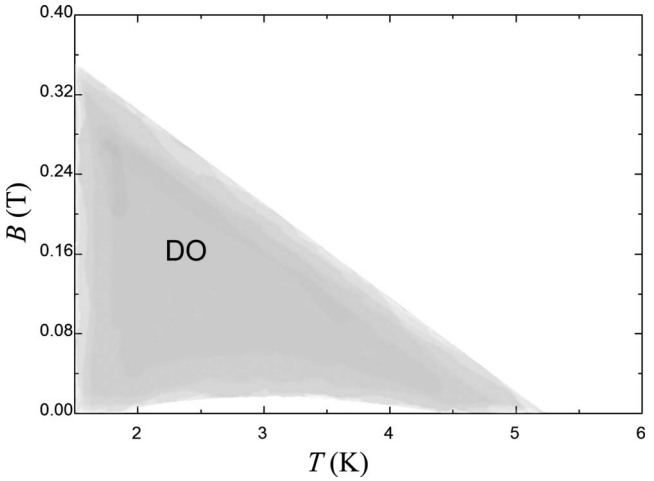

FIG. 6. B-T phase diagram in which the grayed region (DO) corresponds to the occurrence of the peak in R_d vs *I*.

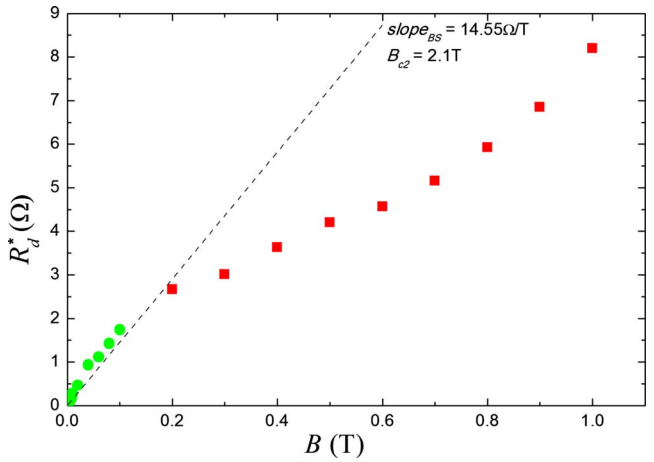

FIG. 7. (Color online) Flux-flow dynamic resistance R_d^* as a function of the external magnetic field at $T=4.2$ K.

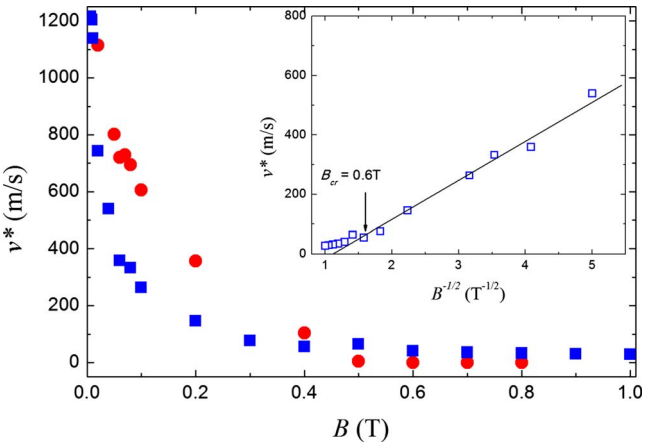

FIG. 8. (Color online) The critical vortex velocity as function of the external magnetic field at 4.2 K (squares), and 2.1 K (circles). Inset: the high field crossover at $B_{cr}=0.6$ T can be identified.

dence of any dynamic melting phase transition such as predicted in Ref. 12 and usually observed instead for weaker pinning materials, such as Nb-Ge (Ref. 13) and Mo-Ge.[16]

In the region of the B-T plane where DO occurs, in the limit of large electric currents, above the maximum of the slope dV/dI and just below the instability at the critical vortex velocity v^*, the slope of the IVC's is expected to be only little affected any more by flux pinning. This means that the dynamic pinning force can be considered current independent. Hence, in this current regime the IVC's can provide some information on "free flux flow." In Fig. 7 the experimental dynamic resistance at 4.2 K is plotted as function of B: the full dots represent the slopes $dV/dI=R_d^*$ just before the instability. The dynamic resistance R_d^* is seen to increase monotonically with increasing B. At magnetic fields lower than 0.2 T the resistance R_d^* increases about linearly with the flux density B, the functional form is close to, although not identical with the BS prediction, thus $R_d^* \approx R_{BS}$.

For an intermediate field range (0.2 T$<B<$1.0 T) the slope of R_d^* vs B becomes smaller than the BS prediction. For magnetic fields above the DO region (see Fig. 6) the dynamical resistance increases monotonically with the current until the instability takes place. At higher fields ($T=4.2$ K, $B>1.5$ T), as B_{c2} is approached, the instability disappears [see Fig. 2(b)]: the voltage jump turns into a continuous increase of the voltage toward the normal state value and the actual value of the flux-flow resistance cannot be identified by the dynamical resistance anymore. This latter increase has been previously observed and appears to be typical of the flux-flow resistance close to B_{c2} in type-II superconductors.[37] For a quantitative comparison with the BS prediction, in Fig. 7 we also show the plot of R_nB/B_{c2} (dashed line), in reasonable agreement with the experimental data at low fields. Here R_n is the resistance value measured above T_c at 10 K, and the value $B_{c2}(4.2\ \mathrm{K})=2.1$ T was taken by the criterion $J_c=0$ A/cm^2 in the measured $J_c(B,T)$ dependence. Some deviations of the differential resistance from the expected BS prediction have been already reported on different materials that also display the disorder driven dynamic transition in the flux-flow state.[38,39] Moreover, there exists a large intermediate magnetic-field range where the experimental curve falls below the values calculated from BS. A similar behavior has been recently reported for the case of a multilayer Ta/Ge sample.[40] However, this will be addressed in a different paper.

Regarding the experimental results at very low magnetic fields, an estimate of the self-field B_{self} of the applied electric current I is important. Taking the value $I=0.3$ A [from Fig. 2(a)] and the geometric cross section of the Nb film, one finds $B_{self}=2$ mT. This value indicates that the self-field remains sufficiently small to be neglected in our discussion.

IV. FLUX-FLOW INSTABILITY

The IVC shown in Figs. 1(a) and 2(a) display the abrupt voltage jumps which are the fingerprint of the flux-flow instability. In Fig. 8 the critical vortex velocity v^* is plotted versus the magnetic flux density B for the temperatures of 2.1 and 4.2 K. At magnetic fields larger than about 0.6 T the critical velocity v^* is nearly independent of B, whereas at lower magnetic fields it increases with decreasing B.

The independence of the critical flux-flow velocity v^* of the magnetic field above about 0.6 T, shown in Fig. 8, agrees with the LO theory.[25] However, this theory assumes spatial homogeneity of the nonequilibrium quasiparticle distribution. This spatial homogeneity requires that the critical velocity v^* multiplied by the quasiparticle energy relaxation time τ_ϵ must reach at least the intervortex distance $a_0 \sim 1/B^{1/2}$. As has been discussed in Ref. 41, this leads to a crossover effect between a regime with a constant value of v^* at high magnetic fields and a regime with $v^* \sim 1/B^{1/2}$ at lower magnetic fields. In the inset of Fig. 8 this crossover can clearly be seen.

According to Eq. (2) the energy relaxation time τ_ϵ can be calculated from the critical vortex velocity v^*. In Fig. 9 we show a typical plot of v^* versus the reduced temperature obtained at the magnetic flux density $B=0.01$ T. The critical vortex velocity is seen to be nearly independent of the temperature below about $t=0.7$. This independence of the temperature suggests the dominance of quasiparticle scattering by lattice defects,[30,42] which seems reasonable. The reduction

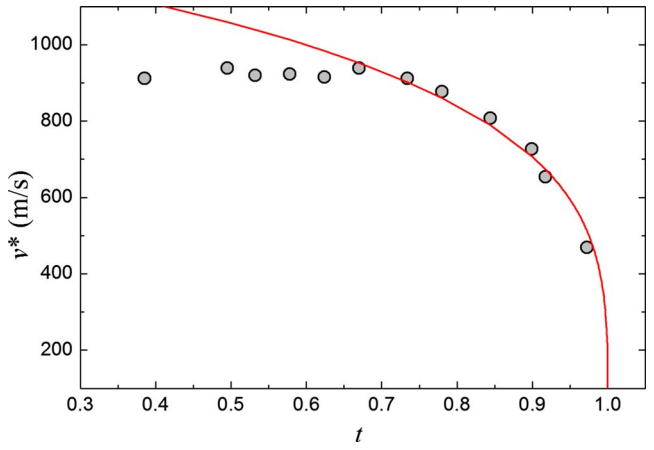

FIG. 9. (Color online) Temperature dependence of critical vortex velocity at $B=0.01$ T. The solid line is the fitted curve based on the LO prediction of Eq. (2).

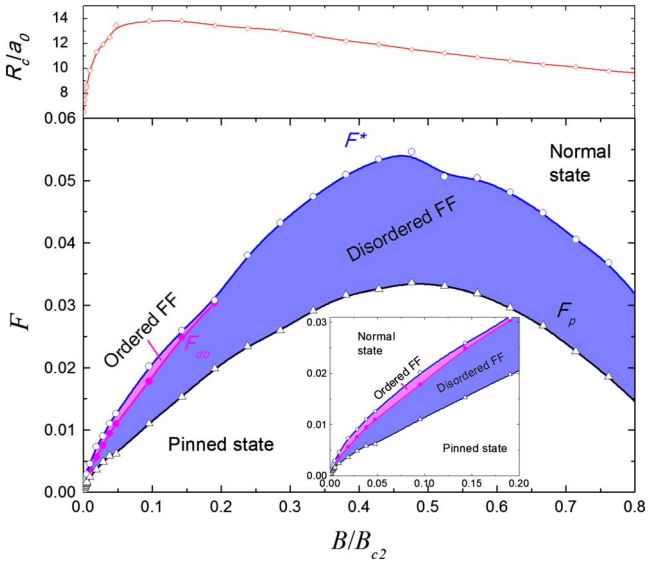

FIG. 10. (Color online) F-B phase diagram at $T=4.2$ K. On the upper panel the correlation length R_c/a_0 is shown.

of v^* above $t=0.7$ appears to be associated with the factor $(1-T/T_c)^{1/4}$ in Eq. (2).[27] From the results such as shown in Fig. 9 one finds the value of about $\tau_\epsilon \approx 5.0\times 10^{-10}$ s, in agreement with the literature,[42,43] independent of the temperature in the range above about $t=0.7$.

Starting from the obtained energy relaxation time τ_ϵ, we are able to verify the validity of the condition $v^*\tau_\epsilon = a_0$, which ensures the spatial homogeneity of the nonequilibrium quasiparticle distribution. Since $a_0=(2\Phi_0/\sqrt{3}B)^{1/2}$ is magnetic-field dependent, whereas τ_ϵ is assumed constant within the LO theory, and we directly measured the critical vortex velocities $v^*(B)$ (see Fig. 8), we find that such condition is always satisfied for fields $B \leq B_{cr}$.

V. DYNAMIC PHASE DIAGRAM

In our Nb samples, due to the fairly strong intrinsic pinning, we were able to detect both the disorder driven dynamic transition and the flux-flow instability of the moving vortex lattice. On one side, dynamic ordering results from the competition between the moving elastic vortex lattice and the strength of the pinning centers. Indeed, within the collective pinning (CP) theory,[44] we can assure that our samples belong to the two-dimensional (2D) CP case, since the condition $L_c > d/2$ is satisfied with $L_c \approx 3[b/(1-b)]^{1/2}R_c$.[45] According to 2D CP, a short range order is retained within the correlated volume V_c, whose correlation lengths are $R_c = a_0 c_{66}/F_p^{1/2}$,[45] and L_c, perpendicular and along the field direction, respectively, where c_{66} is the shear modulus.[46]

On the other side, the instability of the moving vortex lattice is affected by the degree of ordering of the flux lattice. From the experimental *I-V* data (see Figs. 1 and 2), we observe the linear flux-flow branches more pronounced in the temperature and magnetic-field range of the DO. This implies that higher flux-flow velocities are needed to reach the highest limit of the critical vortex velocity before the instability drives the system to the normal state. Since it has already been established that DO occurs if a driving force density F_{DO} is larger than the pinning force density F_p,[13] here we can confirm that DO occurs if $F_p < F_{DO} < F^*$, where the force $F^* = I^* B$ is related to the instability current value I^*, and $F_{DO} = I_p B$, where I_p is the value marked by a sharp peak in $R_d(I)$, and $F_p = I_c B$. Therefore, taking these values from the experimental data, we have constructed a dynamic phase diagram in terms of a force-magnetic field diagram (F-B), as shown in Fig. 10 for $T=4.2$ K.

In order to distinguish among the different dynamic flux-flow (FF) states, it is well known that in the region of DO, the disordered vortex lattice starts initially a plastic motion which turns into an elastic flow driven by sufficiently high bias currents. Thus above F_{DO} the whole system is likely more ordered and we have identified it with an "ordered FF." This is confirmed by the magnetic-field dependence of the correlation length R_c.[45] In fact R_c increases up to its maximum value within the magnetic-field range in which DO occurs, as displayed in Fig. 10. At higher fields, above the DO region, R_c becomes a decreasing function of B and F_p is still increasing, as shown in Fig. 10, so that in the absence of a current induced dynamic ordering, the disordered vortex lattice keeps moving in a "disordered FF," although the amount of the disorder can still change in the vortex lattice. Finally, regardless of the applied magnetic field, below the F_p line the lattice is in the pinned state, while the F^* line establishes the limit of stability of the moving vortex lattice above which the system undergoes an abrupt transition to the normal state.

In Fig. 11 we show the dynamic phase diagram at $T=2.1$ K. The main features found at $T=4.2$ K are confirmed. There is a small window in which the ordered flux-flow (OFF) state is established. However, in a wide intermediate magnetic-field range the difference F^*-F_p drops to zero. This is a consequence of the stronger pinning at lower temperatures, so that the amount of the disorder increases and the instability current decreases until $F^*=F_p$.

The role of the increasing disorder on the current induced ordering dynamic transition has been considered in a theo-

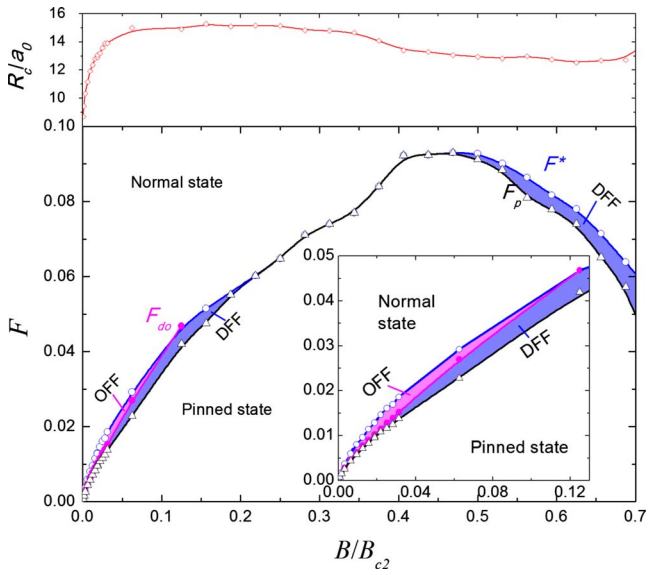

FIG. 11. (Color online) F-B phase diagram at $T=2.1$ K. On the upper panel the correlation length R_c/a_0 is shown. OFF and DFF indicate the ordered and the disordered flux-flow regions, respectively.

retical phase diagram I-B, see Fig. 4 of Ref. 47, in which a sharp dynamic transition is identified in the case of intermediate pinning in the material, due to the presence of large domains of an ordered vortex lattice. This is indeed our case, in which the domain size is found in the range $6a_0-15a_0$, as shown in Figs. 10 and 11, even larger than the strong pinning limit reported as a few times a_0,[17] and smaller than in the case of the weak-pinning materials studied in the past.[13,48] Therefore, although our J_c values are almost four decades larger than in weak-pinning materials, since the magnetic-field range in which DO occurs is around mT (see Fig. 6) compared to the tesla range for the weaker samples, numerically our R_c/a_0 values become comparable with the weaker ones, but the magnetic-field dependence looks like quite different, with the maximum shifted to lower fields since our $F_p(B)$ have a maximum at fields higher than $B/B_{c2}=0.3$. The intermediate pinning regime of our Nb thin films allows us to analyze both the nonlinear effects of the dynamic ordering and the flux-flow instability, and this is the first time such effects have been observed on the same material. Indeed in a recent study on strong pinning Nb thin films,[42] although the flux-flow instability has been carefully investigated, no such current induced DO transition has been reported. In this paper a crystallization phase transition from a plastic flow $J<J_c$ to a moving vortex crystal for $J>J_c$ is proposed. At still higher currents a linear flux flow is always observed with no inflection point until the instability is reached.

VI. CONCLUSIONS

We study the nonlinear flux-flow behavior in the moderately strong pinning Nb superconductor. The experimental shapes of the *I-V* characteristics measured in thin Nb strips reflect the nonlinear feature of the vortex dynamics. In particular, in some field and temperature ranges an S-shape of the flux-flow branch, corresponding to a peak in the flux-flow differential resistance (sensitive to the external magnetic field and temperature) appears, as usually observed only in weak-pinning materials. It can be accounted for in terms of the transition from a disordered vortex phase to an ordered one (i.e., the dynamic ordering) of the moving vortex lattice driven by the bias current. The different values of the effective pinning forces in the different phases determine two different vortex velocities, so that the flux-flow motion is characterized by slower and faster moving vortices. By increasing the bias current, all vortices can reach the same high velocity, and the usual linear flux-flow motion is restored. Nevertheless, in an intermediate magnetic-field range the dynamic resistance cannot be identified anymore with the BS flux-flow resistance.

Once the high velocity regime is achieved, the vortex lattice undergoes a second transition, but this is an abrupt change known as a flux-flow instability, that leads the system to the normal state. The magnetic field and temperature dependences of such critical vortex velocity have been studied within the nonequilibrium theory of Larkin-Ovchinnikov, thus deducing the quasiparticle energy relaxation time τ_ϵ. The electronic nature of the flux-flow instability has been confirmed.

To summarize, a dynamic phase diagram has been proposed to describe the observed flux-flow dynamics arising from the competition between the disorder driven transition and the instability of the moving vortex lattice. These two nonlinear effects manifest themselves in the case of intermediate pinning strength, since a larger disorder can hide the dynamic ordering. On the other side, in the limited temperature and magnetic-field range of the DO, such disorder driven transition can lead to a more stable motion of the vortex lattice. Indeed, this moderately strong pinning regime induces a plastically deformed vortex lattice already for small applied magnetic fields, so that the DO occurs for fields lower than the expected ones in the case of well known weak-pinning materials.

ACKNOWLEDGMENTS

We acknowledge the fabrication of the samples from A. Angrisani Armenio. We are grateful to C. Attanasio for useful discussions. Thanks to D. Zola for reading the paper.

*Corresponding author; grimaldi@sa.infn.it

[1] Y. B. Kim, C. F. Hempstead, and A. R. Strnad, Phys. Rev. **139**, A1163 (1965).
[2] J. Bardeen and M. J. Stephen, Phys. Rev. **140**, A1197 (1965).
[3] R. P. Huebener, R. T. Kampwirth, and A. Seher, J. Low Temp. Phys. **2**, 113 (1970).
[4] R. P. Huebener, O. M. Stoll, and S. Kaiser, Phys. Rev. B **59**, R3945 (1999).
[5] R. P. Huebener, *Magnetic Flux Structures in Superconductors*, 2nd ed. (Springer, Berlin, 2001).
[6] W. H. Warnes and D. C. Larbalestier, Cryogenics **26**, 643 (1986).
[7] A. B. Pippard, Philos. Mag. **19**, 217 (1969).
[8] J. Lefebvre, M. Hilke, and Z. Altounian, Phys. Rev. Lett. **102**, 257002 (2009).
[9] X. B. Xu, H. Fangohr, X. N. Xu, M. Gu, Z. H. Wang, S. M. Ji, S. Y. Ding, D. Q. Shi, and S. X. Dou, Phys. Rev. Lett. **101**, 147002 (2008).
[10] M. G. Adesso, D. Uglietti, R. Flukiger, M. Polichetti, and S. Pace, Phys. Rev. B **73**, 092513 (2006).
[11] M.-O. Andrè, M. Polichetti, H. Pastoriza, and P. H. Kes, Physica C **338**, 179 (2000).
[12] A. E. Koshelev and V. M. Vinokur, Phys. Rev. Lett. **73**, 3580 (1994).
[13] J. M. E. Geers, C. Attanasio, M. B. S. Hesselberth, J. Aarts, and P. H. Kes, Phys. Rev. B **63**, 094511 (2001).
[14] M. C. Faleski, M. C. Marchetti, and A. A. Middleton, Phys. Rev. B **54**, 12427 (1996).
[15] S. Bhattacharya and M. J. Higgins, Phys. Rev. Lett. **70**, 2617 (1993).
[16] M. C. Hellerqvist, D. Ephron, W. R. White, M. R. Beasley, and A. Kapitulnik, Phys. Rev. Lett. **76**, 4022 (1996).
[17] T. D. Luccio, C. Attanasio, A. Andreone, and A. M. Cucolo, Eur. Phys. J. B **25**, 263 (2002).
[18] S. Bhattacharya and M. J. Higgins, Phys. Rev. B **49**, 10005 (1994).
[19] W. R. White, A. Kapitulnik, and M. R. Beasley, Phys. Rev. B **50**, 6303 (1994).
[20] Y. Paltiel, Y. Myasoedov, E. Zeldov, G. Jung, M. L. Rappaport, D. E. Feldman, M. J. Higgins, and S. Bhattacharya, Phys. Rev. B **66**, 060503(R) (2002).
[21] L. Balents and M. P. A. Fisher, Phys. Rev. Lett. **75**, 4270 (1995).
[22] A.-C. Shi and A. J. Berlinsky, Phys. Rev. Lett. **67**, 1926 (1991).
[23] K. Moon, R. T. Scalettar, and G. T. Zimanyi, Phys. Rev. Lett. **77**, 2778 (1996).
[24] S. Ryu, M. Hellerqvist, S. Doniach, A. Kapitulnik, and D. Stroud, Phys. Rev. Lett. **77**, 5114 (1996).
[25] A. I. Larkin and Y. N. Ovchinnikov, Sov. Phys. JETP **41**, 960 (1976).
[26] G. Grimaldi, A. Leo, A. Nigro, S. Pace, A. A. Armenio, and C. Attanasio, J. Phys.: Conf. Ser. **97**, 012111 (2008).
[27] G. Grimaldi, A. Leo, A. Nigro, S. Pace, C. Cirillo, and C. Attanasio, Physica C **468**, 765 (2008).
[28] M. N. Wilson, *Superconducting Magnets*, edited by R. G. Scurlock (Oxford University Press, New York, 1983).
[29] A. Bezuglyj and V. Shklovskij, Physica C **202**, 234 (1992).
[30] G. Grimaldi, A. Leo, C. Cirillo, C. Attanasio, A. Nigro, and S. Pace, J. Phys.: Condens. Matter **21**, 254207 (2009).
[31] Z. L. Xiao, P. Voss-de Haan, G. Jakob, T. Kluge, P. Haibach, H. Adrian, and E. Y. Andrei, Phys. Rev. B **59**, 1481 (1999).
[32] E. J. Kramer, J. Appl. Phys. **44**, 1360 (1973).
[33] A. Leo, Ph.D. thesis, Univesità degli Studi di Salerno, 2009.
[34] R. G. Jones, E. H. Rhoderick, and A. C. Rose-Innes, Phys. Lett. **24A**, 318 (1967).
[35] B. Brown, Phys. Rev. B **61**, 3267 (2000).
[36] N. Kokubo, R. Besseling, and P. H. Kes, Phys. Rev. B **69**, 064504 (2004).
[37] Y. B. Kim and M. J. Stephen, *Superconductivity* edited by R. D. Parks (Marcel Dekker, New York, 1969), Vol. 2, p. 1107.
[38] S. Bhattacharya and M. J. Higgins, Phys. Rev. B **52**, 64 (1995).
[39] P. Berghuis, A. L. F. van der Slot, and P. H. Kes, Phys. Rev. Lett. **65**, 2583 (1990).
[40] B. J. Ruck, J. C. Abele, H. J. Trodahl, S. A. Brown, and P. Lynam, Phys. Rev. Lett. **78**, 3378 (1997).
[41] S. G. Doettinger, R. P. Huebener, and A. Kühle, Physica C **251**, 285 (1995).
[42] C. Peroz and C. Villard, Phys. Rev. B **72**, 014515 (2005).
[43] A. Angrisani Armenio, C. Bell, J. Aarts, and C. Attanasio, Phys. Rev. B **76**, 054502 (2007).
[44] A. I. Larkin and Y. N. Ovchinnikov, J. Low Temp. Phys. **34**, 409 (1979).
[45] R. Wordenweber and P. H. Kes, Phys. Rev. B **34**, 494 (1986).
[46] E. H. Brandt, Rep. Prog. Phys. **58**, 1465 (1995).
[47] M. Chandran, R. T. Scalettar, and G. T. Zimanyi, Phys. Rev. B **67**, 052507 (2003).
[48] P. H. Kes and C. C. Tsuei, Phys. Rev. B **28**, 5126 (1983).